A Structural Theory for Non-stoicheiometry. Part 4.† Defect Fluorite-type Structures: Vacancy Superstructures in Ordered Calcium Oxide–Hafnium Dioxide Ternary Oxides

By **Bernard F. Hoskins**, Department of Inorganic Chemistry, University of Melbourne, Parkville, Victoria, Australia 3052

Raymond L. Martin *‡ and **Donald Taylor**, Research School of Chemistry, Australian National University, P.O. Box No. 4, Canberra, Australia 2600

The structures of each of the known ternary phases of the $CaO–HfO_2$ system are interpreted in terms of the co-ordinated defect (c.d.) model. In all the three phases the integrity of the c.d. is retained with an essential aspect being the cation centring of c.d.s along $\langle 111\rangle_F$ directions. The Φ_1-$Ca_2Hf_7O_{16}$ phase is based on a close-packed arrangement of isolated $[111]_F$ related metal-centred pairs of c.d.s which occupy only one third of the $(111)_F$ anion layers. For the Φ_2-$Ca_6Hf_{19}O_{44}$ phase each $[111]_F$-related metal-centred pair of c.d.s is connected to two further pairs along other $\langle 111\rangle_F$ directions, forming helices of c.d.s throughout the structure. The c.d.s are confined to prisms of sesquioxide composition $M_2O_3[CaHfO_3\square]$ which are separated from each other by intersecting $\{1\bar{1}0\}_F$ planes of composition HfO_2. The Φ-$CaHf_4O_9$ phase has been shown to be comprised of a complex system of intergrowths involving three previously unrecognised distinct phases, one of which also has the overall parent composition $CaHf_4O_9$ while the other two have the new stoicheiometries $CaHf_6O_{13}$ and $CaHf_2O_5$. Even for the regions of the most reduced phase, $CaHf_2O_5$, the c.d. remains intact by the subtle overlaying of $(100)_F$ strips of $CaHf_2O_5$ with domains of the more oxidised phases. The analysis has suggested that, as well as the unique topological requirements of the c.d., both cation ordering and the retention of a three-fold axis of symmetry from the parent fluorite structure are important structure-determining features of Φ-$Ca_2Hf_7O_{16}$ and other defect fluorite-related oxide phases.

THE occurrence of ordered intermediate phases with fluorite ($C1$)-related structures in the ternary mixed-oxide systems $CaO–HfO_2$,[1-4] $CaO–ZrO_2$,[5] and $Sc_2O_3–ZrO_2$ [6-9] is well established. The crystal structures of the phases $CaHf_4O_9$, $Ca_2Hf_7O_{16}$, and $Ca_6Hf_{19}O_{44}$ have been determined recently from a combination of X-ray powder intensity measurements and unit-cell data derived from electron-diffraction patterns given by single-crystal fragments of these phases.[10,11] All the three phases are superstructures derived from the defect-fluorite structure by the ordering of vacant anion sites. The evidence for concomitant ordering of the cations is unambiguous in the phases of the $CaO–HfO_2$ system,[10,11] but this aspect remains uncertain for the $ZrO_2–Sc_2O_3$ phase, $Zr_{10}Sc_4O_{26}$.[8]

The direct location of anion vacancies by the refinement of the occupancies of the anion sites poses a problem in the structure analysis because of the small contribution of the oxygen atoms to the overall X-ray intensity data. However, the more accurate structure determinations of the type C-lanthanoid sesquioxide,[12,13] ι-Pr_7O_{12},[14] $Zr_3Yb_4O_{12}$,[15] $Zr_{10}Sc_4O_{26}$,[8] and $Ca_2Hf_7O_{16}$ [10] provide convincing evidence that a necessary consequence of creating an anion vacancy is an expansion of the encapsulating tetrahedron of metal atoms. Thus, in C-type In_2O_3 [12] the tetrahedron edge for an OIn_4 octant is 3.52 Å compared with 3.83 Å for that of $\square In_4$. This observation provides a useful structural probe for determining which of the anion sites are most likely to be unoccupied in defect fluorite-type oxides.

In the previous paper,[16] superstructures of the fluorite lattice which characterise the ordered phases (n = 7, 9, 10, 11, and 12) in the homologous series Pr_nO_{2n-2} were interpreted in terms of the concept of the co-ordination defect (c.d.).[17] In particular, topological arguments enabled structural relations between the triclinic (odd n) and monoclinic (even n) homologues to be suggested. The ordered phases in the $CaO–HfO_2$ and $Sc_2O_3–ZrO_2$ systems offer an opportunity to ascertain whether the c.d. concept can be extended usefully from binary to ternary phases. A recent analysis of the $Sc_2O_3–ZrO_2$ system [18] has revealed that its known structures can be successfully accounted for in terms of the c.d. model so that, in this paper, attention will be focused on the new structures reported for phases of the $CaO–HfO_2$ system. Of particular significance is the well defined ordered cation system which is a characteristic of each phase and which is in direct contrast to the statistical distribution of the metal atoms reported for the phases of the

† Part 3 is ref. 16.

‡ *Present address:* Monash University, Clayton, Victoria, Australia 3168.

[1] C. Delamarre and M. Perez y Jorba, *Compt. rend.*, 1965, **261**, 5128.
[2] C. Delamarre and M. Perez y Jorba, *Rev. Int. Hautes Temper. et Refract.*, 1965, **2**, 313.
[3] C. Delamarre, *Rev. Int. Hautes Temper. et Refract.*, 1972, **9**, 209.
[4] J. G. Allpress, H. J. Rossell, and H. G. Scott, *Mat. Res. Bull.*, 1974, **9**, 455.
[5] D. Michel, *Mat. Res. Bull.*, 1973, **8**, 943.
[6] J. Lefevre, *Ann. Chim. (France)*, 1963, **8**, 117.
[7] R. Collongues, F. Queyroux, M. Perez y Jorba, and J.-C. Gilles, *Bull. Soc. chim. France*, 1965, 1141.
[8] M. R. Thornber, D. J. M. Bevan, and J. Graham, *Acta Cryst.*, 1968, **B24**, 1183.
[9] M. R. Thornber, D. J. M. Bevan, and E. Summerville, *J. Solid State Chem.*, 1970, **1**, 545.
[10] H. J. Rossell and H. G. Scott, *J. Solid State Chem.*, 1975, **13**, 345.
[11] J. G. Allpress, H. J. Rossell, and H. G. Scott, *J. Solid State Chem.*, 1975, **14**, 264.
[12] M. Marezio, *Acta Cryst.*, 1966, **20**, 723.
[13] M. G. Paton and E. N. Maslen, *Acta Cryst.*, 1965, **19**, 307.
[14] R. B. von Dreele, L. Eyring, A. L. Bowman, and J. L. Yarnell, *Acta Cryst.*, 1975, **B31**, 971.
[15] M. R. Thornber and D. J. M. Bevan, *J. Solid State Chem.*, 1970, **1**, 536.
[16] B. F. Hoskins and R. L. Martin, *J.C.S. Dalton*, 1976, 676.
[17] R. L. Martin, *J.C.S. Dalton*, 1974, 1335.
[18] R. L. Martin, *J. Proc. Roy. Soc. New South Wales*, 1976, **109**, 137.

Sc_2O_3–ZrO_2 system. One further important aspect of the CaO–HfO_2 system concerns the nature of the metal atoms involved. Whereas, for example, in the binary praseodymium–oxygen system rapid electron transfer between the Pr^{3+} and Pr^{4+} cations can occur, the oxidation state of calcium in its ternary oxide systems must remain invariant at two. Accordingly, it may be anticipated that the ordering of the cation lattice in the CaO–HfO_2 phases could play a dominant role in determining the positioning of the vacant anion sites in the superstructures. Hence, it becomes essential to ascertain whether the structural integrity of the c.d., $M_{3.5}\square O_6$, with its own unique structure-determining character is maintained in these phases. Also, it is important to determine whether the c.d.s are distributed throughout the superstructures as isolated units or as metal-centred pairs each with the composition $M_7\square_2O_{12}$.

Although it has been proposed [10] that the ordered phase $Ca_2Hf_7O_{16}$ conforms to the general framework of fluorite-related M_nO_{2n-2} (*i.e.* with $n = 9$) phases which characterise the binary praseodymium + oxygen system, the existence of $CaHf_4O_9$ and $Ca_6Hf_{19}O_{44}$ suggest that this analogy is fortuitous. The substitution of Ca for Hf in HfO_2 introduces a vacancy in the oxygen lattice, and from the point of view of their composition the known phases conform to a new homologous series $Ca_nHf_{3n+1}O_{7n+2}\square_n$ where $n = 1$, 2, and 6. It will emerge, however, that the nature of at least one of these phases, Φ_1–$CaHf_4O_9$, is indeed more complex than this general formula would suggest and, for this reason, the discussion relating to the Φ_1 phase will be considered last.

The Φ-$Ca_2Hf_7O_{16}$ *Phase.*[10]—The unit cell of Φ-$Ca_2Hf_7O_{16}$ is rhombohedral with space group $R\bar{3}$, and its volume is 2.25 times that of the fluorite sub-cell from which it is derived. The Ca and Hf atoms are ordered on the cation sites of the sub-cell with the Ca atoms segregated on to every third cation layer parallel to the $(111)_F$ plane, each of which has the composition Ca_2Hf. Evidence for ordering of the formal anion vacancies derives from the dilation of the cation tetrahedra which enclose a vacancy. The rhombohedral cell contains six vacant oxygen sites per unit cell, all of which are situated along the rhombohedral three-fold axis of symmetry. The three axes of the rhombohedral cell are related to the parent fluorite lattice according to the transformations:

$$a_1 = \tfrac{1}{2}a_F + b_F + \tfrac{3}{2}c_F$$

$$a_2 = \tfrac{3}{2}a_F + \tfrac{1}{2}b_F + c_F$$

$$a_3 = a_F + \tfrac{3}{2}b_F + \tfrac{1}{2}c_F$$

Compositionally, this phase is identical with the $n = 9$ member of the homologous series of the binary praseodymium oxides ζ-Pr_9O_{16}, although, in fact, it seems to be the $n = 2$ member of the apparent series $Ca_nHf_{3n+1}O_{7n+2}\square_n$. In order to compare these two structures it is convenient to define the location of vacant anion sites in terms of the c.d. concept. The distribution of c.d.s in each $(100)_F$ octant layer of the ternary phase is shown in Figure 1(*a*) with adjacent layers displaced by the vector $\frac{1}{2}[150]_F$; for convenience the axes have been chosen to conform with the cubic orientations employed in Part 3.[16] The mating holes (H) designate unfilled octants within a $(100)_F$ layer which are filled by the octants which project from c.d.s comprising the adjoining layers. The small cross-hatched squares represent octants of the fluorite unit cell of composition $M_{0.5}O$. Since the rhombohedral unit cell is oblique (α 38.8°), eighteen $(100)_F$ layers must be superimposed along a_F to define the true unit cell.

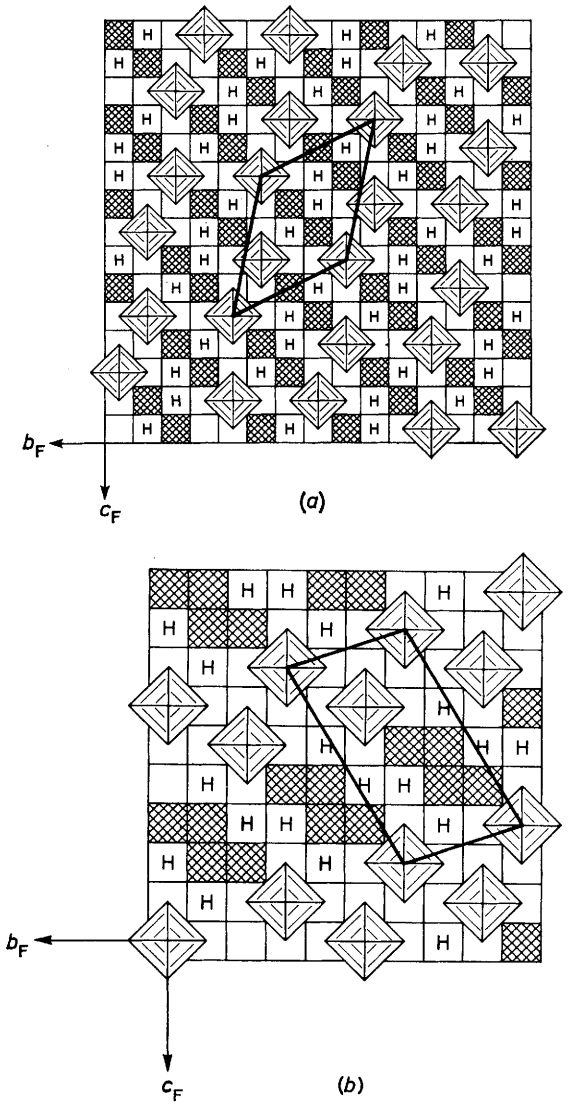

FIGURE 1 (*a*) Idealised square-matrix representation of a $(100)_F$ octant layer of the Φ-$Ca_2Hf_7O_{16}$ lattice showing the location of vacant oxygen sites; a structural repeat unit is outlined in in black. The adjacent layer is displaced by the vector $\frac{1}{2}[150]_F$. (*b*) The pattern of c.d.s in a typical layer of the ζ-Pr_9O_{16} structure

Each vacant anion site is in an environment of six oxygen atoms disposed approximately at the corners of an octahedron with four hafnium atoms located at the corners of an interpenetrating tetrahedron. A feature of the structure is that the anion vacancies are arranged in

metal-centred pairs with the overall composition of the ι-phase, *i.e.* $Hf_7O_{12}\square_2$. The central hafnium atom is six-co-ordinate and the remaining six hafnium atoms are seven-co-ordinated by oxygen. The composition of the ι-phase is achieved since each metal-centred pair of c.d.s is associated with four octants, each of composition $Ca_{0.5}O$ with the calcium atoms always retaining the full eight-co-ordination of the parent fluorite structure. The metal-centred pairing of c.d.s again occurs along the $[111]_F$ direction noted previously but, unlike ζ-Pr_9O_{16},

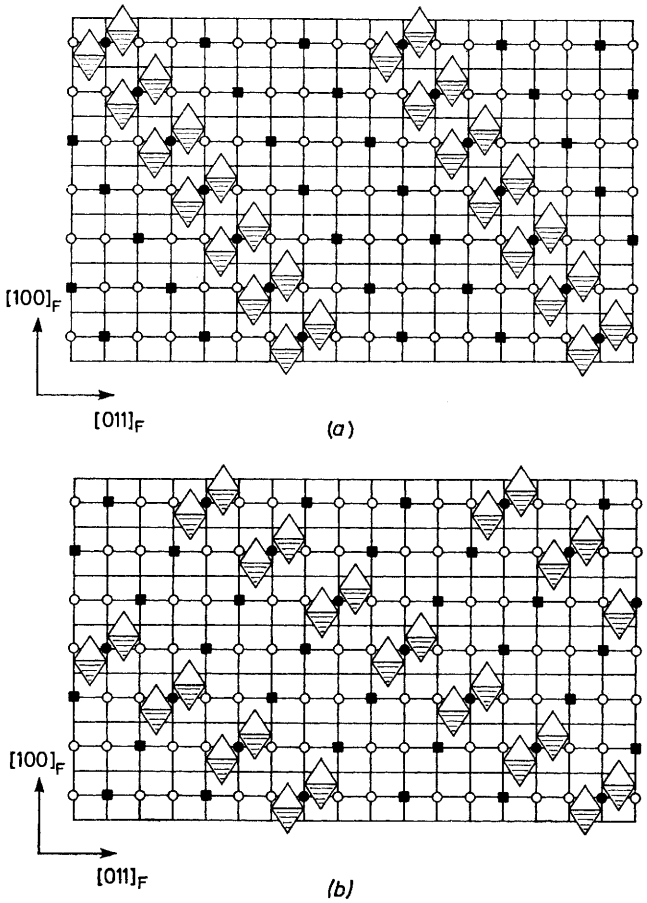

FIGURE 2 Structure of (*a*) Φ-$Ca_2Hf_7O_{16}$ and (*b*) ζ-Pr_9O_{16} shown on $(01\bar{1})_F$ planes. Metal atoms with co-ordination numbers of six, seven, and eight are marked as ●, ○, and ■ respectively

the pairs are distributed evenly throughout the lattice, rather than being gathered into clusters and columns along the $[21\bar{1}]_F$ direction.

The ordered arrangement of c.d.s in a $(100)_F$ layer of $Ca_2Hf_7O_{16}$ [Figure 1(*a*)] can be compared with a corresponding layer of ζ-Pr_9O_{16} [Figure 1(*b*)]. Although certain directional relations between anion vacancies are common to both structures (*e.g.* $[111]_F$, $[012]_F$, $[11\bar{2}]_F$, *etc.*), the superlattices differ in both symmetry and size. There appears to be no simple structural operation which relates the two structures, although it is possible to convert a $(100)_F$ layer of ζ-Pr_9O_{16} into one of Φ-$Ca_2Hf_7O_{16}$ by the consecutive shear operations [031][01$\bar{1}$] and [015][011]. Other important structural features of Φ-$Ca_2Hf_7O_{16}$ are readily apparent from the consideration

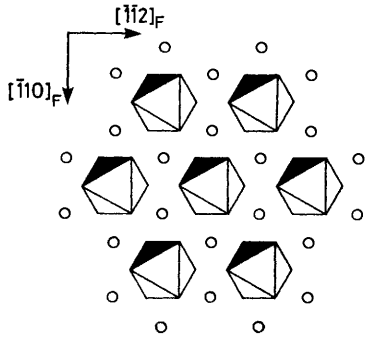

FIGURE 3 The arrangement of vacant anion sites on every third $(111)_F$ plane of Φ-$Ca_2Hf_7O_{16}$ showing their anion co-ordination polyhedra

of the $(01\bar{1})_F$ planes, each of which has an identical distribution of cation and vacant anion sites. This is shown, together with a corresponding plane of the binary phase ζ-Pr_9O_{16}, in Figure 2(*a*) and 2(*b*), and this reveals that the arrangement of the $[111]_F$ metal-centred pairs along the $[2\bar{1}\bar{1}]_F$ direction for Φ-$Ca_2Hf_7O_{16}$ is fundamentally different from the $[21\bar{1}]_F$ distribution of metal-centred pairs of ζ-Pr_9O_{16} which is not contained in the plane.

The highest concentration of vacancies in $Ca_2Hf_7O_{16}$ is found in the $(111)_F$ planes. Vacancies are segregated on to every third $(111)_F$ oxygen plane which has the composition $\{\square O_2\}_n$, *i.e.* 33⅓% of the anion sites are empty. This value may be compared with the corresponding $(111)_F$ planes of type *C*-Pr_2O_3 (*cf.* ref. 19, Figure 9) and ι-Pr_7O_{12} where the corresponding figures are 25 and 14.3%, respectively. In fact, it will be evident from Figure 3 that this represents the most compressed arrangement of c.d.s possible in a $(111)_F$ layer without corner- or edge-sharing being involved. Each vacancy-containing plane is sandwiched between oxygen-intact planes to yield the arrangement of c.d.s illustrated in Figure 3. This may be compared with the

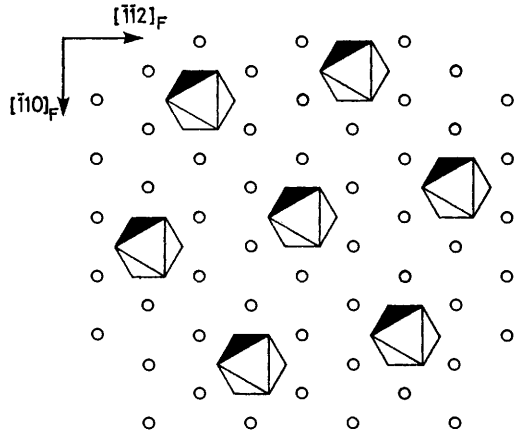

FIGURE 4 A typical $(111)_F$ plane of ι-Pr_7O_{12}

more expanded arrangement of c.d.s found in the $(111)_F$ vacancy-containing planes of ι-Pr_7O_{12} (Figure 4).

[19] B. F. Hoskins and R. L. Martin, *J.C.S. Dalton*, 1975, 576.

It has already been noted that for this phase the vacancies, the arrangement of which is shown in Figure 3, are confined to only one type of anion plane in the cubic close-packed arrangement of $(111)_F$ metal and oxygen layers, the sequence of which is $B_oA_oB_mC_oB_oC_m$-$A_oC_oA_mB_oA_o$, *etc.* If, say, the vacancies are confined to the A-type anion layers, the vacancy arrangement throughout the structure is such that the vacancy patterns on any pair of adjacent A-type anion layers which sandwich an A-type metal layer directly overlay each other, and it is this arrangement of vacancies and metal atoms, together with the appropriate oxygen-intact planes, which gives rise to the independent $[111]_F$-related metal-centred pairs of c.d.s. In the three-dimensional structure the $(111)_F$ laminae of $[111]_F$-related metal-centred c.d. pairs are themselves arranged in an A, B, C, *etc.*, sequence, *i.e.* the metal-centred c.d. pairs can be regarded as forming a cubic close-packed array throughout the structure.

The segregation of vacant anion sites on to selected $(111)_F$ anion planes is a most striking feature of the rhombohedral Φ-$Ca_2Hf_7O_{16}$, particularly when it is possible to construct a rhombohedral phase of the general composition $M_9\square_2O_{16}$ with each $(111)_F$ anion layer possessing an identical trigonal arrangement of vacant oxygen sites, *i.e.* with each $(111)_F$ anion plane having the composition $[\square O_8]$.

The Φ_2-$Ca_6Hf_{19}O_{44}$ *Phase.*[11]—The unit cell, its relation to the fluorite-type sub-cell, and its symmetry have been determined by electron diffraction from single-crystal fragments of this phase together with *X*-ray powder data. This phase possesses a rhombohedral cell, space group $R\bar{3}c$, and the three axes of the rhombohedral cell are related to the parent fluorite lattice according to the transformations:

$$a_1 = -a_F + \tfrac{3}{2}b_F + \tfrac{3}{2}c_F$$

$$a_2 = \tfrac{3}{2}a_F - b_F + \tfrac{3}{2}c_F$$

$$a_3 = \tfrac{3}{2}a_F + \tfrac{3}{2}b_F - c_F$$

An examination of the location of vacant anion sites in this phase confirms that each is invariably co-ordinated by six nearest oxygen neighbours so that the c.d. representation can be employed to visualise the superstructure. The arrangement of c.d.s in a $(100)_F$ layer is illustrated in Figure 5. The structure and composition of the Φ_2-phase is obtained by stacking successive $(100)_F$ layers of octants of the fluorite cube, the contiguous layers being displaced relative to each other by the vector $\frac{1}{2}[116]_F$ or $\frac{1}{2}[161]_F$. It is clear from the location of the mating holes H that pairing of c.d.s occurs along $\langle 111\rangle_F$ directions. This relation emerges more clearly if the superstructure is considered in terms of $(01\bar{1})_F$ fluorite planes.

The Φ_2-phase is composed of three types (A, B, and C) of $(01\bar{1})_F$ plane arranged in the sequence ABCCBABCCB . . ., *etc.* Plane A contains no oxygen vacancies. However, planes B and C both contain anion vacancies and have the compositions $Ca_4Hf_6O_{16}\square_4$ and $Ca_2Hf_8O_{18}\square_2$, respectively. When combined with the plane A of composition $Hf_{10}O_{20}$, the composition of the Φ_2-phase $Ca_{12}Hf_{38}O_{88}\square_{12}$ is obtained. The arrangement of c.d.s in the planes B and C is illustrated in Figure 6(*a*) and 6(*b*) respectively. The c.d.s are not isolated but are linked by metal-centred pairing: for the B-type plane, pairing along $[111]_F$ and $[\bar{1}11]_F$ gives rise to quartets of c.d.s which run along $[\bar{2}33]_F$, *i.e.* the directions of $a_{rhomb.}$. The density of c.d.s of the C-type planes is half that of the B-type, and the arrangement of c.d.s for the C-type planes can be regarded as a derivative of the B-type by the regular omission of alternate $[111]_F$ paired c.d.s along the $[\bar{2}33]$ direction.

It is instructive to consider the structure of Φ_2-$Ca_6Hf_{19}O_{44}$ in terms of its sequence of $(111)_F$ anion planes. Relative to fluorite-type MO_2, each $(111)_F$ layer

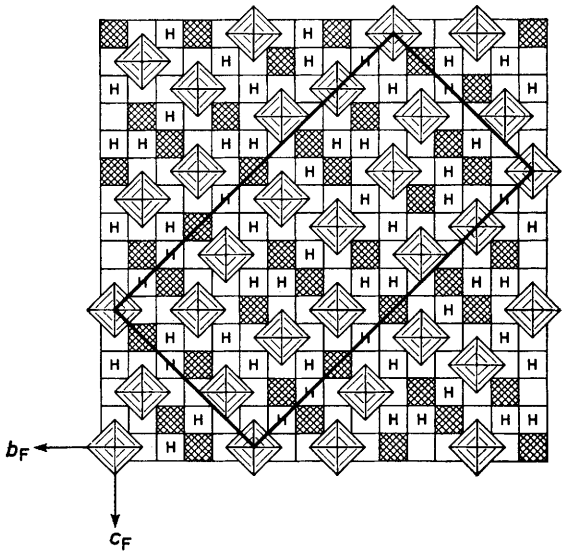

FIGURE 5 Distribution of c.d.s in a $(100)_F$ octant layer of Φ_2-$Ca_6Hf_{19}O_{44}$. The adjacent layer is displaced by the vector $\frac{1}{2}[116]_F$ or $\frac{1}{2}[161]_F$

of oxygen atoms has $\frac{3}{25}$ of the oxygen positions vacant to yield the stoicheiometry $\square_3O_{22}$. The anion vacancies are organized so that each is octahedrally co-ordinated by oxygen to preserve the $\square O_6$ entity. The c.d.s in each layer are clustered in triangular groups of three, with the clusters themselves forming the fundamental motif of the hexagonal representation of the $(111)_F$ layer; these aspects are shown in Figure 7(*a*). Allpress *et al.*[11] pointed out that the structure contains discrete $\{1\bar{1}0\}_F$ sheets of composition HfO_2 which do not contain anion vacancies. These sheets divide the structure into triangular prisms parallel to $[111]_F$ within which all the departures from the fluorite structure and composition occur.

These features are revealed if $(111)_F$ anion planes of the type illustrated in Figure 7(*a*) are stacked with the appropriate $(111)_F$ metal planes in the sequence $B_oA_oB_m$-$C_oB_oC_mA_oC_oA_mB_oA_o$, *etc.*, to yield the element of structure which is depicted in the insert portion of Figure 7(*a*). This diagram may be compared with Figure 1(*a*) of

Allpress *et al.*[11] in which the broken lines indicate the projection of sheets of perfect fluorite composition HfO_2

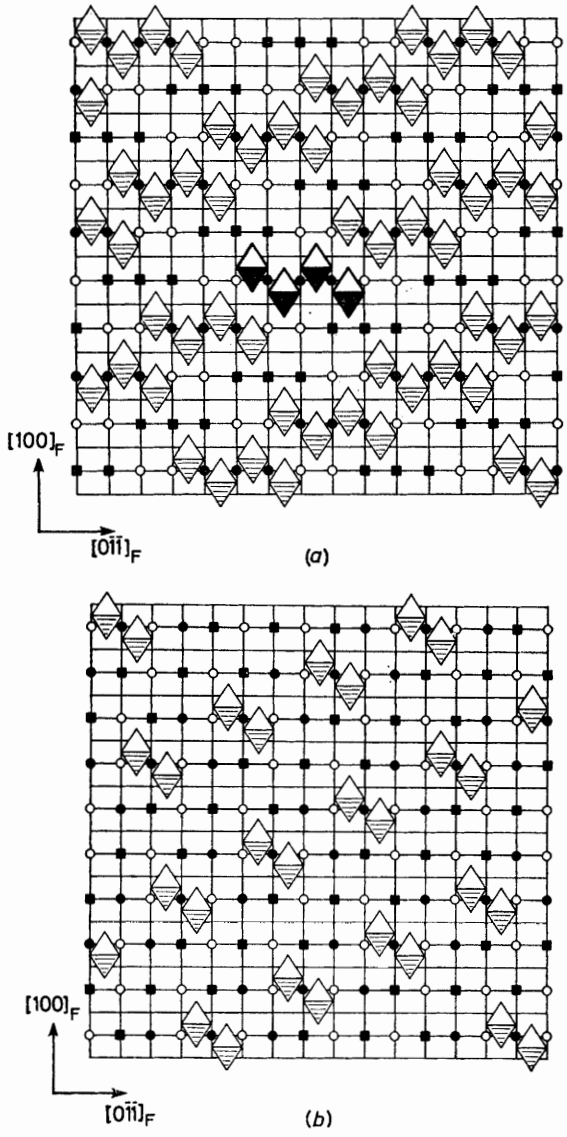

FIGURE 6 Arrangement of vacant anion sites on $(01\bar{1})_F$ planes for (*a*) type B planes of composition $Ca_4Hf_6O_{16}\square_4$ and (*b*) type C planes of composition $Ca_2Hf_8O_{18}\square_2$. Metal atoms with co-ordination numbers of six, seven, and eight are marked as ●, ○, and ■. One of the quartets of c.d.s in plane B is darkenened

and the full lines outline the prisms containing metal ions and anion vacancies. Within the insert of Figure 7(*a*) the small triangles of c.d.s outline in projection three of the six prisms which occur in this element of structure. The c.d.s occur on $(111)_F$ planes at the levels with $(24z_{hex.})/c_{hex.} = 1, 3, 9, 11, 17, 19, 25$, *etc.* and contain the metal-centred vectors $\langle 111\rangle_F$ which define the helical chain along the $[111]_F$ direction. Metal-centred pairing of the $[111]_F$ type occurs between the c.d.s centred on any pair of adjacent $(111)_F$ layers of the same cubic close-packed type between which lies a $(111)_F$ metal layer of this type and this is true for all three types of $(111)_F$ layers. However, the c.d. pairs formed in this fashion are not isolated because further metal-centred pairing occurs between each c.d. of a $[111]_F$ related pair and a c.d. of another $[111]_F$ related pair along one of the

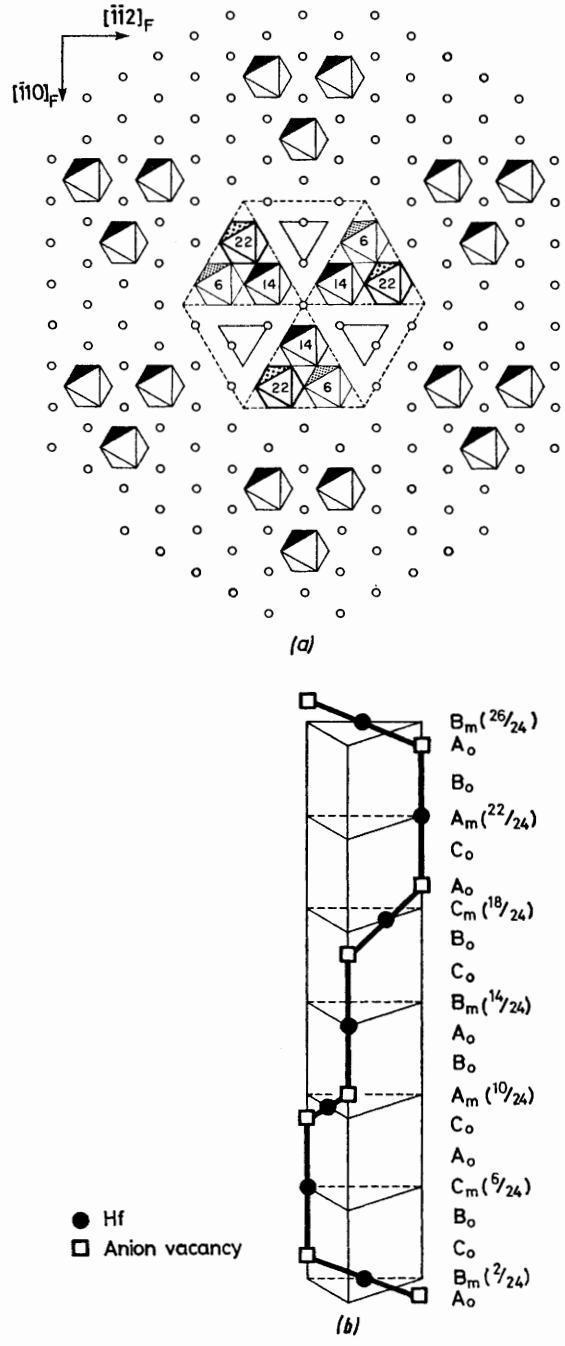

FIGURE 7 (*a*) A section of the Φ_2-$Ca_6Hf_{19}O_{44}$ structure perpendicular to the $[111]_F$ axis showing the arrangement of vacant anion sites. The broken lines outline a hexagonal element of structure which is formed by the projection of sheets of perfect fluorite of composition HfO_2 on to a $(111)_F$ plane at $(24\ z_{hex.})/c_{hex.} = 11$. This element of structure contains six triangular prisms of the type shown in (*b*) which gives the elevation of one triangular prism. For the c.d.s shown, metal-centred pairing occurs along $[111]_F$ at the levels $(24\ z_{hex.})/c_{hex.} = 6$, 14, 22, *etc.* as indicated in (*b*)

remaining $\langle 111\rangle_F$ directions, which leads to the spiral effect already noted. This is illustrated in the insert in Figure 7(*a*) which shows in projection the total contents of a prism with each of the octahedra actually representing the projection of $[111]_F$ related metal-centred pairs of c.d.s. For the three prisms illustrated, the levels of the $(111)_F$ metal layers on which the metal atoms of the $[111]_F$ pair of c.d.s occur with $(24z_{hex.})/c_{hex.} = 6$, **14**, **22**, *etc.*, and the values over one unit-cell length are shown for the relevant c.d. pairs in Figure 7(*a*). An alternative view of this prism is depicted in Figure 7(*b*). This shows the stacking sequence of the $(111)_F$ metal and oxygen planes, together with the $(z_{hex.}/c_{hex.})$ values of the c.d.s and the metal atoms involved in the $[111]_F$ pairing. In Figure 7(*b*), the coalescence of the $[111]_F$-related c.d. pairs by further metal centring along each of the remaining $\langle 111\rangle_F$ directions is readily seen together with the arrangement and relative orientations of the hafnium-centred vacancy pairs within the prism. The c.d.s which define the prism represented by the unfilled triangles of the insert of Figure 7(*a*) occur at the remaining levels, *i.e.* with $(24z_{hex.})/c_{hex.}$ values of **5**, **7**, **13**, **15**, **21**, **23**, **29**, *etc.*, and these are likewise related by $\frac{1}{2}\langle 111\rangle_F$ vectors.

It is interesting to note that the composition of each prism is $Ca_6Hf_6O_{18}\square_6$ corresponding to that of a sesquioxide. When combined with the intersecting fluorite sheets of composition $Hf_{13}O_{26}$ the overall composition of the Φ_2–phase is obtained. It should be noted that, like the type *C*-M_2O_3 structure,[19] the prisms contain all the possible $\langle 111\rangle_F$ vectors between metal-centred c.d.s.

The Φ_1-$CaHf_4O_9$ *Phase.*[11]—It has been found that Φ_1-$CaHf_4O_9$ has the most complex structure of the known ternary CaO–HfO_2 oxides. As with the other phases discussed in this paper, the unit-cell dimensions of this phase, its symmetry, contents, and relation to the fluorite sub-cell have been determined from electron-diffraction studies of single-crystal fragments together with *X*-ray powder data. This phase possesses a monoclinic cell, space group *C*2/*c*, with the three axes related to the parent fluorite axis according to the transformations:

$$a_m = 2a_F + 2b_F + 2c_F$$
$$b_m = -2a_F + 2b_F$$
$$c_m = -\tfrac{3}{2}a_F - \tfrac{3}{2}b_F + c_F$$

Although the overall composition conforms to the $n = 10$ member of the homologous series M_nO_{2n-2}, the distribution of vacant anion sites appears to be completely different to that of ε-$Pr_{10}O_{18}$. The composition of the Φ_1-phase also suggests that it can be regarded as the $n = 1$ member of the series $Ca_nHf_{3n+1}O_{7n+2}\square_n$; however, the true nature of this phase is very much more complex than this generalisation indicates.

As for the Φ-$Ca_2Hf_7O_{16}$ and Φ_2-$Ca_6Hf_{19}O_{44}$ phases, the integrity of the c.d. is maintained for Φ_1-$CaHf_4O_9$ and the distribution of vacant anion sites in a $(100)_F$ anion layer is illustrated in Figure 8. It can immediately be seen that the distribution of c.d.s appears to be very much more complex than that observed for either the Φ or Φ_2 phase. However, a closer inspection reveals that the c.d. distribution can be resolved into three distinct and uniform regions of different composition and finite width with the overall structure and composition of the Φ_1 phase being obtained by the stacking of successive

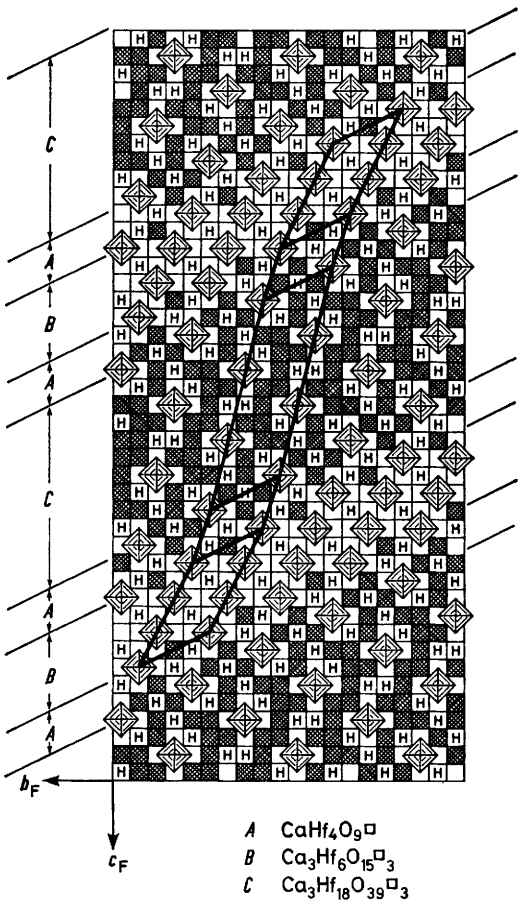

FIGURE 8 Distribution of c.d.s in a $(100)_F$ octant layer of Φ_1-$CaHf_4O_9$ showing coherence at various interfaces between the A, B, and C regions of intergrowth. Contiguous layers are displaced by the vector $\frac{1}{2}[1\bar{3}4]_F$. Elements of structure possessing the appropriate anion vacancy compositions are outlined for several of the discrete structural regions which characterise the Φ_1 phase

$(100)_F$ layers, with contiguous layers displaced relative to each other by the vector $\frac{1}{2}[1\bar{3}4]_F$.

Essentially the Φ_1 phase is comprised of an intergrowth of three regions of composition, one of which has a composition identical to that of the overall composition to the phase, *i.e.* $CaHf_4O_9\square$, while the other two have the compositions $Ca_3Hf_6O_{15}\square_3$ and $Ca_3Hf_{18}O_{39}\square_3$. If these three regions are designated A, B, and C respectively, the $(100)_F$ layer of Φ_1 is comprised of an infinite repetition of these in the sequence ABAC, from which the overall composition is made up as follows: $CaHf_4O_9\square$ + $Ca_3Hf_6O_{15}\square_3$ + $CaHf_4O_9\square$ + $Ca_3Hf_{18}O_{39}\square_3$ = $Ca_8Hf_{32}O_{72}\square_8$ [*i.e.* $(CaHf_4O_9\square)_8$]. It is interesting to note that in earlier papers (*viz.* ref. 17, Figure 11; ref.

19, Figure 13) intergrowths such as the type observed here for Φ_1-$CaHf_4O_9$ have been suggested to account for the more complex regions of the praseodymium–oxygen phase diagram.

A most unexpected result of this analysis has been the observation that one of the three regions which comprise the assemblage of Φ_1, $CaHf_2O_5\square$ ($MO_{1.667}$), is more reduced than the phase generated by the closest packing of c.d.s, *i.e.* $M_{3.5}\square O_6$ ($MO_{1.714}$). The $CaHf_2O_5\square$ phase is compositionally identical to that of Sr_2UO_5; however, the corner-sharing arrangement of c.d.s found for the latter phase [19,20] is not required for Φ_1-$CaHf_4O_9$. It can be seen from Figure 8 that the arrangement of c.d.s in the $CaHf_2O_5$ region is such that there are insufficient mating holes to allow for the contiguous packing of $(100)_F$ layers of the same composition. There is a close relation between the structural elements of $CaHf_2O_5$ and the more oxidised regions, which makes them dimensionally compatible so that intergrowth between the elements in the appropriate sequence can occur coherently at interfaces parallel to the $(11,1,\bar{2})_F$ plane. This accounts for the obliqueness of the plane and the relative band widths of the individual constituent phases. These last two points deserve further comment.

Although the most oxidised and most reduced phases are dimensionally compatible in the $(100)_F$ layer along the $[042]_F$ direction, the trace of $(11,1,\bar{2})_F$ on $(100)_F$, successive $(100)_F$ layers cannot be stacked along $[100]_F$ without the presence of the phase of intermediate composition which ensures that there is a coincidence between mating holes of contiguous $(100)_F$ layers. In fact, the location of the mating holes in the reduced phase determines not only the necessity for the phase of intermediate composition but also its width, because it is the intermediate and reduced phases that overlay each other between contiguous $(100)_F$ layers resulting in the $[1\bar{3}4]_F$ stacking vector. The unusually low symmetry commented on by Allpress *et al.*[11] is not unexpected because, as this analysis of the phase in terms of the c.d. model shows, Φ_1-$CaHf_4O_9$ arises as the coherent intergrowth of three different regions.

It is interesting to note that, when suitable allowance has been made for the appropriate changes in orientation, the c.d. distribution of the $(010)_F$ layers is identical to that of $(100)_F$ suggesting that the Φ_1-phase is derived from two interpenetrating intergrowth systems. There are two types of $(001)_F$ layers and each of these has a much simpler c.d. pattern than does $(100)_F$, but the existence of the intergrowth system is not readily discerned from either type of $(001)_F$ and these will not be considered further.

Allpress *et al.*[11] noted that the vacancies in the Φ_1-phase do not form infinite chains as in Φ_2-$Ca_6Hf_{19}O_{44}$ but occur in runs of four which are separated by three different vectors of the type $\frac{1}{2}\langle 111\rangle_F$ across six-co-ordinate Hf atoms and which can be discerned in the vacancy chains of Φ_2. A close inspection of the mating holes of a $(100)_F$ layer reveals the vector relation existing between the four $\langle 111\rangle_F$ related c.d.s, but the quartet of c.d.s is readily seen from the consideration of the $(011)_F$ layers. Each $(011)_F$ layer has the same composition and pattern of c.d.s. Figure 9 shows the c.d. arrangement in a typical $(011)_F$ layer which can be seen to be developed from a cluster of vacancies which contain groups of three c.d.s which possess the $\frac{1}{2}[1\bar{1}1]_F$ and $\frac{1}{2}[\bar{1}\bar{1}1]_F$ vector relation and the appropriate metal-centred pairing. The quartet of c.d.s arises from the $\frac{1}{2}[\bar{1}11]_F$ relation to a c.d. in the next-but-one layer, which is also across a six-co-ordinate Hf atom, and this is shown by the labelled overlay in Figure 9. The complex intergrowth pattern of c.d.s in $(100)_F$ is not evident in $(011)_F$ layers and an

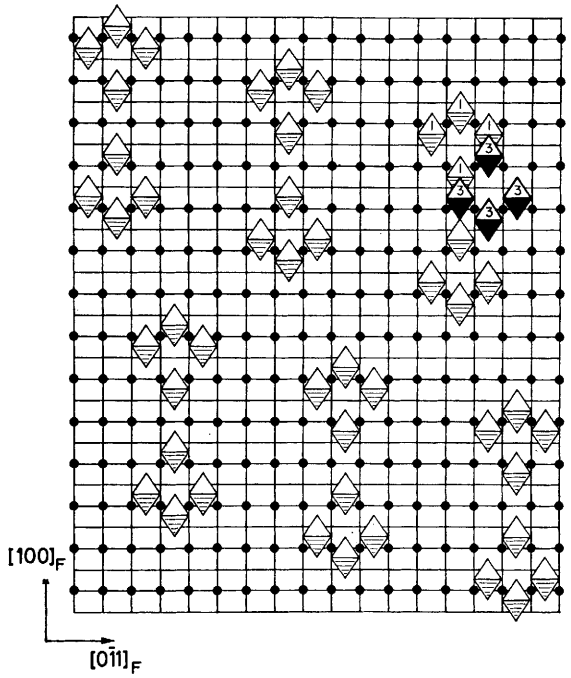

FIGURE 9 Structure of Φ_1-$CaHf_4O_9$ in a typical $(011)_F$ layer. The quartet of c.d.s involving three of the $\langle 111\rangle_F$ vectors is completed by the overlay of layer 1 with layer 3 as shown

orderly motif emerges with a more even distribution of c.d.s, and which is indeed much more uniform than the distribution found for the corresponding planes of the Φ_2-phase.

As indicated by the monoclinic symmetry, the $\{111\}_F$ planes of Φ_1-$CaHf_4O_9$ possess different motifs and all of these possess a lower symmetry than those of either the Φ- and Φ_2-phases. However, the arrangement of c.d.s on a typical $(1\bar{1}\bar{1})_F$ plane is depicted in Figure 10 and this shows the presence of equitriangular groups of c.d.s somewhat suggestive of the pattern that characterises the Φ_2-phase. The basic unit of structure common to all $(1\bar{1}\bar{1})_F$ anion planes is outlined in Figure 10 and this has the required composition $[\square_4O_{36}]$.

Each c.d. of the single line of c.d.s which runs along $[1\bar{3}4]_F$ connects across six-co-ordinate metal atoms to two c.d.s, each belonging to the triangular cluster situated on an adjoining $(111)_F$ layer, to generate three

[20] M. Sterns and J. O. Sawyer, *J. Inorg. Nuclear Chem.*, 1964, **26**, 2291.

of the quartet of metal-centred $\langle 111\rangle_F$-related c.d.s. The fourth member of the quartet lies along the $[1\bar{1}\bar{1}]_F$ direction. The analysis of the Φ_1-$CaHf_4O_9$ phase in terms of its $(1\bar{1}\bar{1})_F$ planes has proved useful in demonstrating that this phase contains embryonic features of the Φ_2-phase. However, the composition of the $(111)_F$ planes does not readily provide information about the true nature of this phase, *i.e.* that it is formed by the intergrowth of three discrete structural regions.

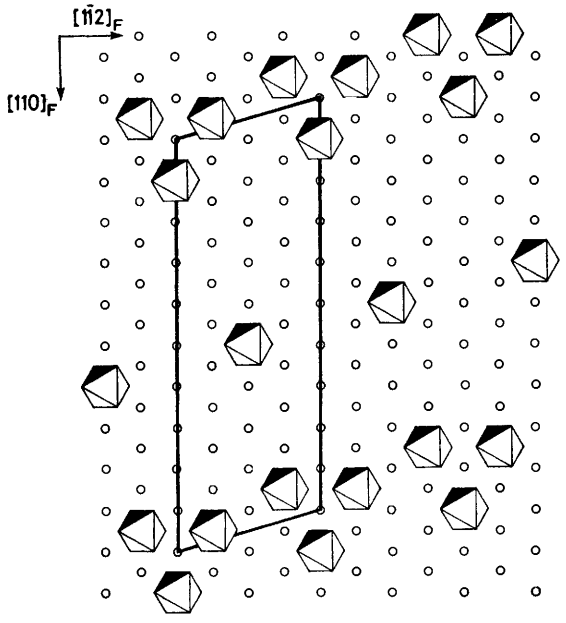

FIGURE 10 Arrangement of c.d.s on a typical $(1\bar{1}\bar{1})_F$ plane of Φ_1-$CaHf_4O_9$

DISCUSSION

It has been found that the structures of the ternary CaO–HfO_2 phases can be readily described in terms of the topological c.d. model proposed [17] for defect fluorite-related oxide systems and we believe that this analysis has thrown new light on the nature of these structures. Again, the c.d. remains intact with the $M_{3\cdot5}\square O_6$ entity being a central feature of all the three structures, and this is so even for the highly reduced phase $CaHf_2O_5$. As has been noted for the Pr–O binary phases,[16] the metal-centred pairing of c.d.s along $[111]_F$ seems to be fundamental to the structures of the known phases of the CaO–HfO_2 system. However, a major point of difference between the binary and ternary systems is the complete absence from the latter of the $[21\bar{1}]_F$ relation existing between the $[111]_F$ metal-centred c.d. pairs which appears to be a characteristic feature of the Pr–O binary phases, with the result that structures of quite different symmetry and dimensions are found for phases of the same metal to oxygen ratio, *viz.* ζ-Pr_9O_{16} and Φ-$Ca_2Hf_7O_{16}$.

In addition, whereas for phases more oxidised than ι-Pr_7O_{12} in the Pr–O system the $[111]_F$ metal-centred c.d. pairs are isolated, the new feature which has emerged from the analysis of the CaO–HfO_2 phases is the linking through metal atoms of metal-centred pairs of c.d.s along other $\langle 111\rangle_F$ directions. This results in the formation of quartets (Φ_1-$CaHf_4O_9$) or helical columns (Φ_2-$Ca_6Hf_{19}O_{44}$) of c.d.s which can be compared with the extended defects observed for the pyrochlore [17] and the C-M_2O_3 [19] structures.

One further point of comparison between the binary and ternary systems is that the detailed description of the CaO–HfO_2 system in terms of the c.d. model has shown the absence of any direct structural relation between the phases, so that the apparent numerical conformity of the phases to the general formula Ca_n-$Hf_{3n+1}O_{7n+2}\square_n$ is an over-simplification and may even be misleading. However, a far more cogent reason is that the topological analysis of these phases in terms of the c.d. model has revealed a complex system of intergrowths for the phase Φ_1-$CaHf_4O_9$ which has been shown to be composed of quite distinct regions whose compositions, $CaHf_2O_5\square$ and $CaHf_6O_{13}\square$, do not conform to the proposed general formula.

It has been mentioned earlier that, in contrast to the binary oxide phases, there is an opportunity for metal ordering in ternary oxide systems which, in fact, is observed in the CaO–HfO_2 phases and this aspect deserves further consideration. The distribution of vacancies and cations in all the three phases is such that the Ca^{2+} cations always retain the full eight-co-ordination of the parent fluorite structure whereas the Hf^{4+} cations exhibit the three co-ordination numbers of six, seven, and eight. The metal centring of pairs of c.d.s invariably involves an Hf^{4+} cation which is, of course, six-co-ordinate. These observations are in keeping with the general rule that large ions tend to occupy the sites with higher co-ordination numbers (*cf.* the approximate values of the ionic radii [21] of Ca^{2+} and Hf^{4+} are 1.14 and 0.85 Å) and it seems that the disparity between the cation radii and their charges may be the driving force for the cation ordering. At this point it is interesting to note that the Ca^{2+} cations in pure CaO exhibit a co-ordination number of six which increases to eight on incorporation into HfO_2 during the synthesis of these ternary oxide phases.

Of particular importance in this discussion is to distinguish, if possible, between the individual roles played by the ordered cation arrays and the topological requirements of the oxygen-co-ordinated vacant sites in the determination of the ultimate structures possessed by these phases. In this connection, it is most interesting to consider further the structural features of the binary phase ζ-$Pr_9O_{16}\square_2$ and those of the ternary oxide Φ-$Ca_2Hf_7O_{16}\square_2$. Each of these defect-fluorite oxides has the same general formula, M_9O_{16}, and it has been mentioned earlier that, although the structure of each is based on metal-centred pairs of c.d.s, the distribution of the vacant sites is not the same and this is readily seen in the $(01\bar{1})_F$ sections depicted in Figure 2(*a*) and 2(*b*). Another very important aspect of these $(01\bar{1})_F$ sections is that they reveal that the distributions of the cation

[21] R. D. Shannon and C. T. Prewitt, *Acta Cryst.*, 1969, **B25**, 925; 1970, **B26**, 1046.

sites in terms of their co-ordination type along $[100]_F$ and $[011]_F$ are precisely the same for each structure. However, adjoining $[011]_F$ strings of metal atoms are displaced relative to one another by different amounts in the two structures and therefore it has been possible to distribute the anion and vacancy sites in two distinct ways. Alternative methods of distributing the vacant sites over the anion sub-lattice must satisfy not only the topological restrictions of the c.d. but also requirements dependent on the distribution of the co-ordination environments of the cations; *i.e.* the cation ordering seems to play a significant role in the determination of the positions of the metal-centred c.d. pairs throughout the structure.

Another interesting aspect of the Φ-$Ca_2Hf_9O_{16}$ phase is that the Ca^{2+} cations are segregated on to every third $(111)_F$-type metal layer in order to achieve the necessary distribution of co-ordination sites throughout the cation sub-lattice. Also, the c.d.s are centred on only one third of the $(111)_F$ anion layers. From the compositions of Ca_2Hf and $\square O_2$ respectively for these particular sets of $(111)_F$ cation and anion planes, it can be seen that the overall structure can readily retain one of the three-fold axes of symmetry of the parent fluorite structure along the $[111]_F$ direction. Although it is possible to achieve this result for the anion sub-lattice without the necessity of segregating the vacant sites, since $(111)_F$ anion planes of composition $\square O_8$ can be ordered to give three-fold axes of symmetry, this is not so for the cation sub-lattice. Here the segregation of the Ca^{2+} ions is a necessary prerequisite for the retention of the three-fold axes of symmetry. It is interesting to note in this connection that there are a number of phases of special stability in both binary and ternary defect fluorite-related oxide systems which preserve a three-fold axis of the parent structure in both the metal and oxygen sub-lattices; particular examples are ι-Pr_7O_{12},[14] *C*-M_2O_3,[12,13] pyrochlore,[22] Zr_{10}-Sc_4O_{26},[8] Φ-$Ca_2Hf_7O_{16}$,[10] and Φ_2-$Ca_6Hf_{19}O_{44}$.[11] This suggests that the three-fold axis of symmetry is a structure-determining feature which is a remnant of the parent cubic close-packed structure and which leads to the lowest possible energy state for the structure. The retention of the three-fold axis of symmetry is only possible for certain composition types, *viz.* $\square O_2$, $\square O_3$, $\square O_7$, $\square O_8$, *etc.*, for the $(111)_F$ anion layers and the analogous cation compositions in the $(111)_F$ metal layers of the ternary phases, and this may well be a reason why phases of other stoicheiometries are more difficult to achieve.

We thank C. D. Pannan for assistance.

[7/1371 *Received*, 27*th July*, 1977]

[22] R. W. G. Wyckoff, ' Crystal Structures,' 2nd edn., Interscience, New York, 1965, vol. 3, p. 439.